

# Magneto-optical probe of antiferromagnetic sub-phases in a $\pi - d$ electronic system

I.Rutel<sup>1</sup>, S. Okubo<sup>2</sup>, H. Ohta<sup>2</sup>, H. Tanaka<sup>3</sup>, H. Kobayashi<sup>3</sup>, J. Brooks<sup>1</sup>

<sup>1</sup>*National High Magnetic Field Laboratory and Physics Department,  
Florida State University, Tallahassee, FL 32310 USA*

<sup>2</sup>*Molecular Photoscience Research Center and Venture Business Laboratory, Kobe University, Kobe, Japan and*

<sup>3</sup>*Institute for Molecular Science, Okazaki, Japan*

(Dated: November 10, 2018)

The highly insulating antiferromagnetic phase of the magnetic- organic conductor  $\lambda - (BETS)_2FeCl_4$  has been probed by resonant mm wave methods vs. magnetic field, temperature, and frequency. Our results show evidence for magnetic sub-phases within the temperature-field phase diagram as previously predicted by Brossard *et al.* [Eur. Phys. J. B 1, 439(1998)].

The discovery of magnetic field induced superconductivity in  $\lambda - (BETS)_2FeCl_4$  [1] has drawn attention to the unusually large  $\pi - d$  electron spin exchange mechanisms[2] in molecular systems where magnetic order in the d electron system strongly influences the behavior of the conducting  $\pi$  electron system. The more general  $\lambda - (BETS)_2Ga_{1-x}Fe_xBr_yCl_{4-y}$  class of organic conductors, with localized magnetic moments at the anion sites, and conduction electrons in the molecular-cation layers, exhibit competition between magnetic, metallic, insulating, and superconducting ground states[3]. The magnetic field dependent phase diagram of the  $\lambda - (BETS)_2FeCl_4$  material is shown in Fig. 1. For  $H = 0$ , and below the Néel temperature[4] ( $T_N = 8$  K),  $\lambda - (BETS)_2FeCl_4$  enters a highly insulating antiferromagnetic (AF) phase[5]. A spin-flop transition to a canted antiferromagnetic (CAF) phase occurs near 1 T, and above 11 T, a paramagnetic metallic (PM) phase appears. At higher magnetic fields (parallel to the the conducting molecular planes), field induced superconductivity (FISC) is stabilized below 5 K between 18 and 45 T[6]. The FISC state involves the cancellation of the exchange field by the external magnetic field. Although the CAF-PM transition is nearly independent of field direction, the PM-FISC transition requires careful alignment of the field in the  $a-c$  molecular planes to avoid orbital dissipation in the superconducting phase.

The main purpose of this work is to focus on the process by which the magnetic field destroys the CAF state. This process has been previously considered theoretically by Brossard *et al.* who use a generalized Kondo lattice model with two d-electron spin sites and four  $\pi$ -electron HOMO bands[5]. The moments involved can arise from the  $Fe^{3+}$  and spin 1/2 conduction electrons, which can interact through RKKY interactions[5]. One key feature of their model was the strong interdependence of the  $Fe^{3+}$  spin configurations with the electronic structure of the conduction electrons, which at the two extremes yields for AF order - an insulator, and for PM order - a finite Fermi surface. From this they predicted that increasing magnetic field could lead to a sequence of different canting angles as the PM phase was approached. The main result of our work, which is in accord with their predic-

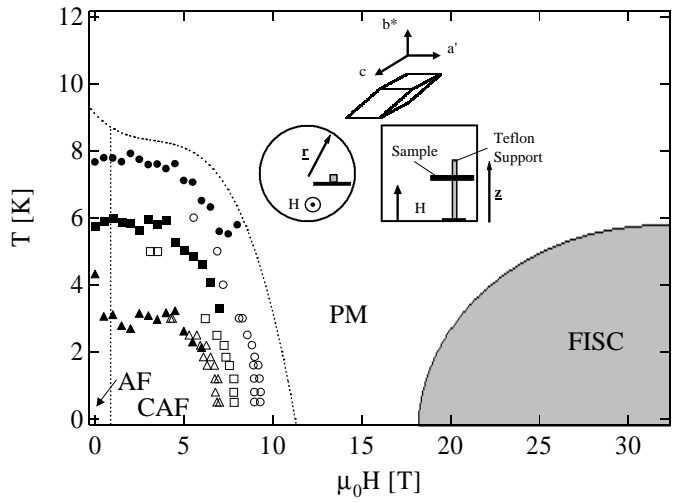


FIG. 1: Phase diagram of  $\lambda - (BETS)_2FeCl_4$ . The four phases identified are antiferromagnetic (AF), canted antiferromagnetic (CAF), paramagnetic metal (PM), and field induced superconducting (FISC) states. Closed (open) symbols represent the temperature (field) sweep measurements of the CAF sub-phase structure: A-circles, B-squares, C-triangles (see text). Schematic: Top figure: sample geometry and principle axes. Lower figures: axial and side views of sample orientation. The sample position shown is for the  $c$ -axis  $\parallel \hat{r}$  and the  $c$ -axis  $\perp \hat{z}$ , where  $\hat{r}$  and  $\hat{z}$  are the unit directions for the axial and radial components of the cylindrical cavity.

tions, is that the CAF spin structure appears to change in steps as the field (and/or temperature) is increased, and that these discrete changes in spin structure cause corresponding steps in the complex conductivity as the PM phase is approached.

Since the resistance below  $T_N$  rapidly becomes unmeasurable, we have probed the antiferromagnetic phase through the use of ac magnetoconductivity, and electron magnetic resonance in the 40 to 110 GHz frequency range. In previous X-band studies[5], the temperature dependent electron spin (ESR) and antiferromagnetic (AFR) resonance features (below  $T_N$ ) have been investigated vs. temperature and sample orientation with respect to magnetic field. In the present study we extend the range of investigation of the CAF state (and also the

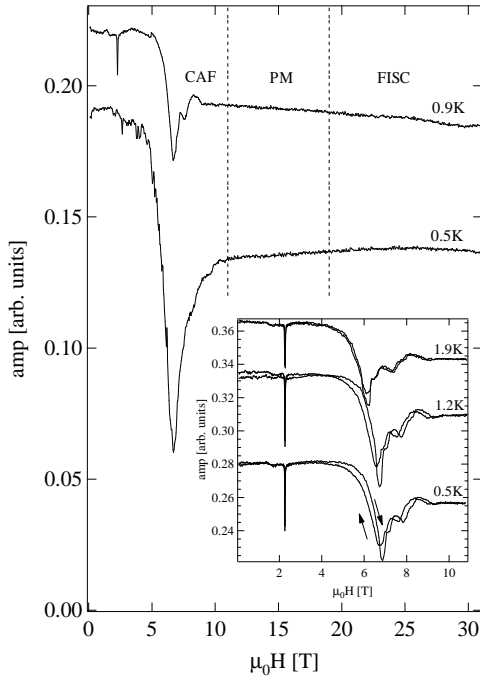


FIG. 2: Low temperature ( $T < T_N$ ) field-dependent mm wave cavity response of  $\lambda - (\text{BETS})_2\text{FeCl}_4$  for  $c \parallel \hat{z}$ ,  $c \parallel \vec{H}$ . (All data is for  $\nu = 66.9$  GHz, except the 0.5 K data in the main panel where  $\nu = 75.4$  GHz.) The sharp dip near 2 T is the ESR line, and the features in the range 5 to 10 T arise from sub-phases in the antiferromagnetic CAF state (see text). Although the sample was aligned to allow the high field superconducting (FISC) state to be stabilized, only weak features associated with a metal to superconducting transition were detected. Inset: Full field sweeps to 11 T. Hysteresis is observed in the sub-phase structure in the CAF state.

FISC state) to a broader range of frequencies, temperatures, and magnetic fields. A mm wave resonant cavity perturbation method is employed[7] where the sample orientation in the cavity can be changed with respect to the field orientation. Samples were synthesized by electrochemical methods[8]. The single crystal used in this work, which was  $0.97 \times 0.10 \times 0.10 \text{ mm}^3$  in size, was greased to a small teflon mount inside the cylindrical cavity resonator. In Fig. 1 the convention for orientation is given in terms of the principle axes of the crystal, and the radial and axial ( $\hat{z} \parallel \vec{H}$  in all cases) unit vectors associated with the cavity. A control experiment insured that the grease and teflon support did not contribute a significant background or spurious ESR signal.

Experiments were carried out in a 30 T resistive magnet and an 8 T superconducting magnet where either temperature or field were held fixed at a specific resonant cavity mode(frequency). A helium 3-probe was modified to allow temperatures down to 0.5 K without interference from liquid dielectric effects. Our results are presented in Figs. 2-5, and the phase diagram of the CAF state, based on all of our results, is shown in Fig. 1. Represen-

tative results are shown for magnetic field sweeps in Fig. 2 for  $c \parallel \hat{z}$  for several temperatures below  $T_N$  up to 30 T. The signal is the phase-locked amplitude of the cavity response, where resonant frequency is allowed to change (via feedback) to keep the phase reference in quadrature. In general, there are two signals in the mm wave cavity response, a resonant signal (i.e.  $h\nu = g\mu B$ ) due to electron spin, and non-resonant structure where there is no functional relationship between frequency and field position. The latter arises from changes in the ac complex conductivity of the material. For increasing field an ESR adsorption line appears, followed by a change in background signal that is punctuated by dips, peaks, and/or shoulders. The field positions of the CAF-PM and PM-FISC phase boundaries observed in transport data are also shown in Fig. 2 for comparison. The features at higher field are not resonant, but reflect step-like changes in the ac magnetoconductivity. As discussed below, we interpret these features as sub-phase transitions in the CAF state for increasing field. An exploration of the high field region where the field induced superconducting phase is stabilized did not show any systematic signature, other than slight, hysteretic loop-like features that were not readily reproducible.

We first address the magnetic resonance data, that is the ESR and AFR measurements used to determine the g-factor and spin-flop field respectively. A temperature dependent investigation of the ESR line, shown in Fig. 3, reveals similar features to those previously reported by Brossard *et al.*, with the g-value exhibiting a non-monotonic temperature dependence below  $T_N$ . The linear frequency-field dependence of the ESR line yielded a g-value of 2.05 for sample orientations away from those where the AFR signal was observable, as shown in Fig. 3b.

For the orientation  $a \parallel \vec{H}, c \parallel \hat{r}$ , we measured the field position of the the AFR signal over our accessible range of frequency, as plotted in Fig. 3b (see also representative trace of data for  $\parallel \vec{H}, c \parallel \hat{r}$  data in Fig. 5 below). Although the frequency dependence of the AFR signal is characteristic of the condition with the field along the hard axis[9, 10, 11, 12], the precise field and magnetic axis relationship is difficult to determine since the easy axis lies about 35 degrees away from the c-axis, and the system is, moreover, canted above the spin flop field. Nevertheless, an extrapolation of the AFR resonance to the zero field gives a gap frequency which corresponds (through  $h\nu/g\mu_B$ ), to a characteristic field of 1.7 T. This value, which is related to the product of the exchange field and the anisotropy field, is comparable to the spin-flop field (1.1 T) reported in magnetization studies[5]. We now turn to the non-resonant features in the ac magnetoconductivity measurements, exhibited in Figs. 2, 4, and 5. We have identified three recurrent features in the temperature and field dependent cavity response below  $T_N$  which appear regardless of frequency or sample ori-

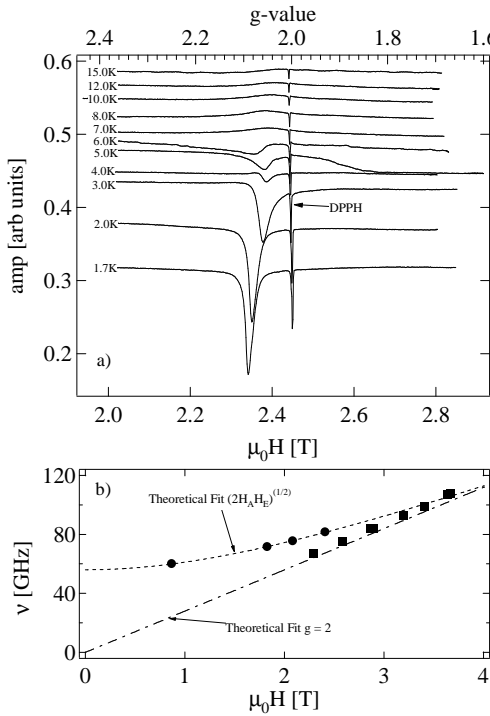


FIG. 3: a) Detailed temperature dependence of the ESR line (with respect to the DPPH marker);  $a \parallel \hat{r}$ ,  $c \parallel \vec{H}$ ,  $\nu = 66.9$  GHz. Below  $T_N$  the g-factor is non-monotonic with decreasing temperature. b) Solid circles - AFR vs. frequency for  $c \parallel \hat{r}$ ,  $a \parallel \vec{H}$ ; Solid squares - ESR vs. frequency for  $c \parallel \hat{z}$ ,  $c \parallel \vec{H}$

tation, labelled as A, B, and C. When plotted vs. T and H, these features are clearly a manifestation of the CAF phase diagram. We interpret these features as changes in the magnetoconductivity of the sample due to changes in the electronic structure in the  $\pi$ -electron system. This can cause changes in the skin depth of the sample and therefore details of the response of the resonant cavity response will change. We cannot, however, at this stage assign these changes to specific values of the complex conductivity of the material.

Fig. 4 shows the temperature dependence of the cavity response for fields between 1 and 8 T. Below 8 K we identify three separate points that indicate a change in the cavity response. As the CAF phase is entered from higher temperatures, the signal is first observed to fall (A), then to rise (B), and then to approach a value after (C) that is larger than that observed above  $T_N$ . The T-H plot of these features, shown in the inset of Fig. 4, follow the general shape of the CAF phase boundary, and indicate the presence of sub-phases. To map out the low temperature sub-phase boundaries we used field sweeps at constant temperature (Figs. 2 and 5). Here, similar structures were identified that allowed extension of the sub-phase transition lines to lower temperatures, as summarized in Fig. 1.

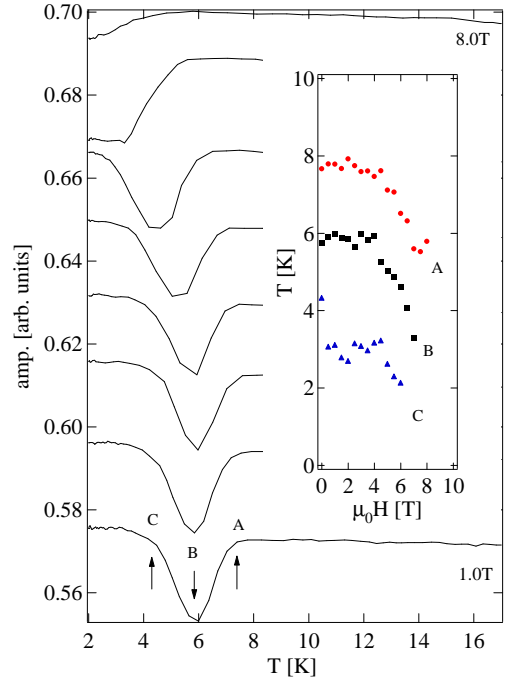


FIG. 4: Temperature dependence of the cavity response at different fields for  $\lambda - (\text{BETS})_2\text{FeCl}_4$ ;  $c \parallel \vec{H}$ ,  $a \parallel \hat{r}$ ,  $\nu = 64.927$  GHz. Three changes in the cavity absorption with temperature are observed at points A, B, and C. Inset: phase boundaries of A, B, and C with temperature and field.

An important point in our interpretation is that the field and temperature position of the features (A,B,C) are non-resonant, and only weakly dependent on sample orientation. Figure 5 serves to demonstrate these assertions, and also sheds further light on the nature of frequency dependent resonant cavity measurements. Here the sample was measured for three different orientations in field, different frequencies, and different temperatures. The ESR line is prominent and absorptive at two of the frequencies, and for  $c \parallel \hat{r}$ ,  $a \parallel \vec{H}$  the AFR signal is observed. Strong ESR or AFR signals are good indications of the sample's coupling to  $\vec{H}_{ac}$ . (A detailed analysis of cavity mode effects will be published elsewhere[13].) In contrast, the ESR line is weak and inverted for the 71.27 GHz data. Here also the field dependence of the background is reversed. It is apparent that the overall signal depends on how the sample is coupled with an  $\vec{E}_{ac}$  or  $\vec{H}_{ac}$  excitation mode, as indicated by the intensity of the ESR features. However, the ESR line positions rigorously follow the linear frequency dependence shown in Fig. 3b. Returning to the non-resonant structures, the appearance of these features depends on the cavity geometry and the resonant mode employed. The dissipation of the cavity is governed by the surface resistance,  $R_s$ , ( $\propto \text{Re} \sqrt{\frac{1}{\sigma}}$ )[14]. The response is a measure of the complex magneto-optical conductivity of the material via the skin depth of the sample,  $\hat{\sigma}$ . Although different shaped

structures appear, their assignments (A, B, or C) on the T-H phase diagram remain congruous. Unlike the ESR lines, these features show no systematic dependence on frequency.

The premise that the spin configuration of the  $Fe^{3+}$  ions affects the electronic structure of the  $\pi$ -electron system has two extremes: the highly insulating AF phase for  $H = 0$ , and the paramagnetic-metallic phase[15] for  $H \gtrsim 11$  T. The energy difference between these two states, based on numerical estimates from the Kondo lattice model[5], is 0.5 meV, or about 6 K, not far from  $T_N$ . Between these two extremes, our data indicate that the electronic structure changes in a step-like manner with either increasing temperature or magnetic field as the CAF-PM state is approached. Since the d- and  $\pi$ -electron spin configuration is a highly coupled system, it is an over simplification to treat the spin projection  $S_Z = \frac{5}{2}$  for the  $Fe^{3+}$  ions as a proper eigenvalue in the relationship  $\mathcal{H} = \frac{-e}{2m_e c} |\mathbf{B}| S_Z$  where  $\mathbf{B}$  is the magnetic field. Although heuristic, we may replace  $S_Z$  with an effective spin  $S_{eff}$  to address the step-wise changes observed in the CAF state. Using the prescription that  $k_B T_{(A,B,C)}(B = 0)$  corresponds to  $\frac{-e}{2m_e c} |\mathbf{B}_{(A,B,C)}| S_{eff}$ , we obtain from Fig. 1 that  $S_{eff} = 0.29, 0.25$ , and  $0.15$  for transitions A, B, and C respectively. This would indicate a stepwise increase in the effective spin projection as the PM phase is approached. Notably,  $S_{eff}$  in the CAF phase is significantly less than  $5/2$ .

In summary, we present new features in the phase diagram of the  $\pi - d$  electron system  $\lambda - (BETS)_2FeCl_4$ . Using a high frequency resonant cavity measurement we show sub-phase structure within the low temperature, low field CAF state. These sub-phase transitions are the result of changes in the spin-configuration in the CAF state which in turn cause changes in the  $\pi$ -electronic structure. These changes are therefore observable as changes in the complex conductivity of the sample in a resonant mm wave cavity. Although stepwise, the transitions are not strictly quantized, and the effective moment is reduced from that of the free d-electron spin. These results are consistent with a highly collective interaction between the  $\pi$ -and d-electron systems.

We are grateful to S. Wiegers, J. Rook, and H. van Luingen for allowing us to use the new Nijmegen-Amsterdam Magnet Laboratory resistive magnet prior to formal commissioning the high field measurements carried out in this work. The authors also acknowledge Venture Business Laboratory, Kobe University. This work is supported by NSF-DMR 99-71474. The mm wave facility was supported through NHMFL/IHRP 5031.

[1] S. Uji, H. Shinagawa, C. Terakura, T. Terashima, T. Yakabe, et al., *Nature* **410**, 908(2001).

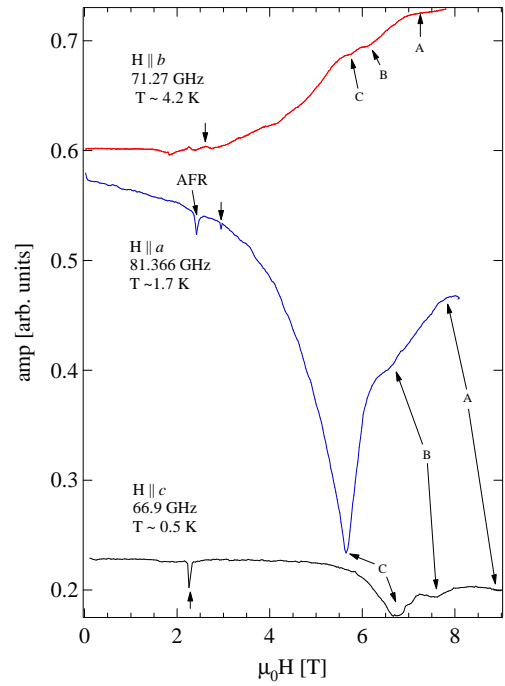


FIG. 5: Magnetic field dependence of cavity response for  $\lambda - (BETS)_2FeCl_4$  in three different sample orientations, frequencies, and temperatures. Arrows indicate the position of the ESR lines, and the AFR line for  $a \parallel \vec{H}$  is also indicated. The step-like structures (A,B, C) between 5 and 10 T appear in all cases.

- [2] T. Mori and M. Katsuhara, *J. Phys. Soc. Japan* **71**, 826-844 (2002).
- [3] H. Tanaka, H. Kobayashi, A. Kobayashi and P. Cassoux, *Advanced Materials* **12**, 1685(2000), and references therein.
- [4] It is not clear at this point if a Peierls-like  $\pi$  electron transition and an antiferromagnetic d-electron transition are, by coincidence, at the same temperature. However, for convenience, in this work we will refer to the transition as  $T_N$ . See also Ref. [3].
- [5] L. Brossard, R. Clerac, C. Coulon, M. Tokumoto, T. Ziman, D. K. Petrov, V. N. Laukhin, M. J. Naughton, A. Audouard, F. Goze, A. Kobayashi, H. Kobayashi, and P. Cassoux, *Eur. Phys. J. B* **1**, 439-452 (1998).
- [6] L. Balicas *et al.*, *Phys. Rev. Lett.* **87**, 067002(2001).
- [7] M. Mola, S. Hill, P. Goy, M. Gross, *Rev. Sci. Inst.* **71**, 1, 1-15 (2000).
- [8] A. Kobayashi, T. Udagawa, H. Tomita, T. Naito, and H. Kobayashi, *Chem. Lett.*, **1993** 2179(1993).
- [9] S. Foner, *Phys. Rev.* **107**, 3, 683-685 (1957).
- [10] M. Hagiwara and K. Katsumata, *RIKEN Review* **24**, 13 (1999).
- [11] C. Coulon, J.C. Scott, and R. Laversanne **33**, 6235 (1986).
- [12] J.B. Torrance, H.J. Pedersen, and K. Bechgaard, *Phys. Rev. Lett.* **49**, 881 (1982).
- [13] S. Okubo, *et al.* to be published.
- [14] S. Hill, J. Brooks, Z. Mao, and Y. Maeno, *Phys. Rev. Lett.* **84**, 15, 3374-3377(2000), and references therein.
- [15] The existence of a quasi-two-dimensional Fermi surface

in the PM phase has been demonstrated by: S. Uji, H. Shinagawa, C. Terakura, T. Terashima, T. Yakabe, Y. Terai, M. Tokumoto, A. Kobayashi, H. Tanaka and H.

Kobayashi, Phys. Rev. B **64**, 024531/5 (2001).